Topochemically controlled Hydrogen Reduction of Scheelite-related Rare-earth Metal Molybdates

By **Jagannatha Gopalakrishnan** * and **Arumugam Manthiram**, Solid State and Structural Chemistry Unit, Indian Institute of Science, Bangalore–560012, India

Scheelite-related α-$Ln_2Mo_3O_{12}$ (Ln = La, Pr, Nd, Sm, Gd, Tb, or Dy) oxides are reduced by hydrogen at 780—870 K yielding molybdenum(IV) oxides of formula $Ln_2Mo_3O_9$. The latter crystallize in a tetragonal scheelite (ABO_4) type structure where one third of the A sites and a quarter of the anion sites are vacant: $Ln_{2/3}(\square cat)_{1/3}MoO_3(\square an)$. The reaction $Ln_2Mo_3O_{12} + 3H_2 \longrightarrow Ln_2Mo_3O_9(\square an)_3 + 3H_2O$ may be regarded as topochemically controlled, since both the parent and the product phases have scheelite-related structures. Infrared spectra and electrical and magnetic properties of these metastable defect scheelite phases are reported.

We have recently reported that the hydrogen reduction of Ln_2MoO_6 to Ln_2MoO_5 (Ln = rare-earth metal) is a topochemically controlled reaction in which the parent and the product oxides have fluorite-related structures.[1] We considered it important to study whether the hydrogen reduction of other rare-earth metal molybdates such as $Ln_2Mo_3O_{12}$ is also topochemically controlled. These molybdates exist in several polymorphic modifications, of which the α forms for Ln = La—Dy crystallize in scheelite-derived structures.[2,3] In the present study, we report the hydrogen reduction of some of these molybdates and characterization of the reduction products by *X*-ray powder diffraction, i.r. spectroscopy, and electrical and magnetic measurements.

Scheelite (ABO_4)-derived molybdates in which the A site is incompletely occupied have been found to be useful catalysts for selective oxidation of olefins.[4] The present study may contribute towards the understanding of these catalytic properties.

EXPERIMENTAL

Rare-earth metal oxides obtained from Indian Rare Earths Ltd. were of >99.9% purity. Molybdenum(VI) oxide was obtained by thermal decomposition of ammonium heptamolybdate (Baker Analysed Reagent) at 750 K. The oxides α-$Ln_2Mo_3O_{12}$ were prepared, as reported in the literature,[5,6] by solid-state reaction between rare-earth metal oxides and MoO_3; the oxides β-$Ln_2Mo_3O_{12}$ were made, as reported by Brixner and co-workers [3,6] and Nassau and Shiever,[2] by heating the α phases above the α–β transition temperatures. The oxides $Ln_2Mo_3O_{12}$ so obtained were reduced in a flowing hydrogen atmosphere at appropriate temperatures (Table 1) for 60—100 h to obtain $Ln_2Mo_3O_9$; the optimum temperature of reduction was determined by monitoring the weight loss. The experimentally found weight losses (Table 1) agree with the values required for reaction (1).

$$Ln_2Mo_3O_{12} + 3H_2 \longrightarrow Ln_2Mo_3O_9 + 3H_2O \quad (1)$$

The oxidation state of molybdenum in the reduction products as determined by oxidimetric analysis [7] (Table 1) is close to IV in conformity with reaction (1). That the composition of the reduction products is actually $Ln_3Mo_3O_9$ was verified by determining the weight gain when reoxidized in air to $Ln_2Mo_3O_{12}$.

The reduction products were characterized by *X*-ray powder diffraction, i.r. spectroscopy, and electrical and magnetic measurements as reported elsewhere.[1,7]

RESULTS AND DISCUSSION

Crystal Chemistry.—*X*-Ray powder-diffraction data (Figure 1 and Table 2) of the products obtained by hydrogen reduction of α-$Ln_2Mo_3O_{12}$ for Ln = La, Pr, Nd, Sm, Gd, Tb, and Dy at 780—870 K together with the chemical analysis results (Table 1) show that stable

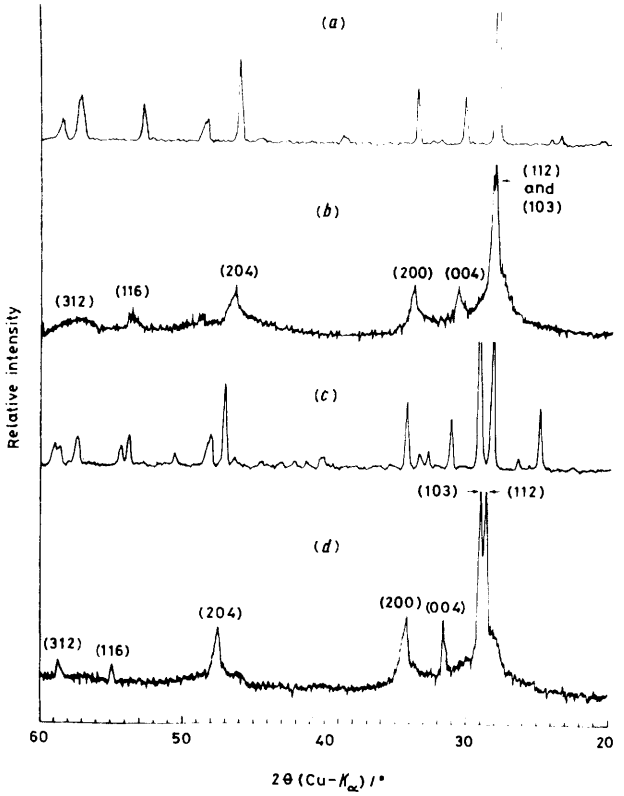

FIGURE 1 *X*-Ray powder diffraction patterns of α-$Ln_2Mo_3O_{12}$ and their reduction products $Ln_2Mo_3O_9$: (*a*) α-$Nd_2Mo_3O_{12}$; (*b*) $Nd_2Mo_3O_9$; (*c*) α-$Gd_2Mo_3O_{12}$; and (*d*) $Gd_2Mo_3O_9$

molybdenum(IV) oxides of formula $Ln_2Mo_3O_9$ are formed. The *X*-ray diffraction patterns of these phases could be indexed on the basis of a tetragonal scheelite cell (Table 2). The cell parameters and their estimated standard deviations (e.s.d.s) are given in Table 1. It is to be noted that all the lines in the patterns could be indexed on a tetragonal scheelite type cell and there are no extra

lines attributable to Ln_2O_3, MoO_2, or MoO_3. The variations of unit-cell parameters and cell volume with the ionic radius of the lanthanide ions [8] are shown in Figure 2. It is seen that, while the cell volume varies continuously, the cell parameters show a discontinuity at samarium. This discontinuity may be due to a difference in the structure of the parent $Ln_2Mo_3O_{12}$ (see later).

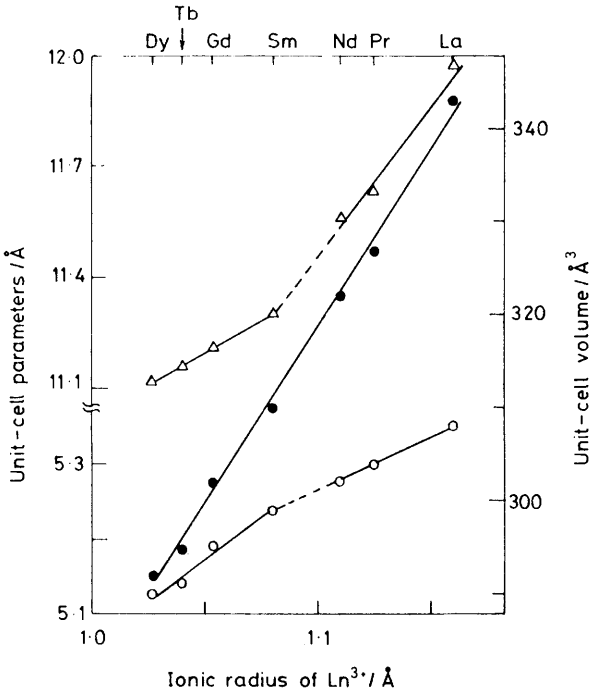

FIGURE 2 Variations of cell parameters [a_T (O), c_T (Δ)] and cell volume [U_T (●)] of $Ln_2Mo_3O_9$ with the radius of the lanthanide ion

The occurrence of the tetragonal scheelite structure for $Ln_2Mo_3O_9$ phases, although surprising at first, may be understood in terms of the structures of the parent $Ln_2Mo_3O_{12}$ oxides. Thus $Ln_2Mo_3O_{12}$ exhibit a complex crystal chemistry showing a variety of polymorphic modifications. The structural aspects of these compounds have been discussed by Brixner and co-workers [3,6] and Nassau and Shiever.[2] For lighter lanthanides (Ln = La, Pr, Nd, Sm, Gd, Tb, and Dy), the α-$Ln_2Mo_3O_{12}$ phases adopt scheelite (ABO_4)-related structures in which the lanthanide ion is co-ordinated to eight oxygens. The composition $Ln_2Mo_3O_{12}$ may be written as $Ln_{2/3}(\square cat)_{1/3}MoO_4$ where □cat denotes an A site vacancy in the scheelite lattice. The A site vacancies are ordered in two different ways: [2,9] on every third of (220) planes of the scheelite structure in the α-$Gd_2Mo_3O_{12}$ (M-type) structure, and a long-range vacancy ordering in the α-$Nd_2Mo_3O_{12}$ (N-type) structure. The α phases of the Sm, Gd, Tb, and Dy compounds crystallize in the M structure while those of La, Pr, and Nd crystallize in the N structure.

The M and N structures of α-$Ln_2Mo_3O_{12}$ are shown in Figure 3 in relation to the ideal ABO_4 scheelite structure.[4,10] It is seen that the former structures are closely related to the ideal structure, except for the monoclinic distortion and the A-site vacancies. The monoclinic supercells of the M and N structures have the following axial relationships with the tetragonal scheelite subcell:

$$\begin{bmatrix} a_M \\ b_M \\ c_M \end{bmatrix} = \begin{bmatrix} 1 & 1 & 0 \\ 0 & 0 & 1 \\ -2 & 1 & 0 \end{bmatrix} \begin{bmatrix} a_T \\ b_T \\ c_T \end{bmatrix}$$

$$\begin{bmatrix} a_{M'} \\ b_{M'} \\ c_{M'} \end{bmatrix} = \begin{bmatrix} -5 & 1 & 0 \\ 0 & 0 & 1 \\ 1 & 2 & 0 \end{bmatrix} \begin{bmatrix} a_T \\ b_T \\ c_T \end{bmatrix}$$

The $Ln_2Mo_3O_{12}$ molybdates of heavier lanthanides and yttrium crystallize in a tetragonal or orthorhombic structure [2,3] in which the lanthanide ions have lower co-ordination numbers (six or seven). It is significant that these non-scheelite $Ln_2Mo_3O_{12}$ yield only *X*-ray amorphous products on hydrogen reduction.

The formation of tetragonal scheelite $Ln_2Mo_3O_9$ phases from α-$Ln_2Mo_3O_{12}$ (M and N structures) is therefore understandable because the parent oxides also have scheelite-derived structures. Reaction (2)

$$Ln_2Mo_3O_{12} + 3H_2 \longrightarrow Ln_2Mo_3O_9(\square an)_3 + 3H_2O \quad (2)$$

(where □an denotes an oxygen vacancy) may be regarded as topochemically controlled,[11] similar to the reduction [1] of Ln_2MoO_6 to Ln_2MoO_5. The removal of monoclinic distortion of the parent lattice on hydrogen reduction is likely to be related to the formation of Mo^{4+} $4d^2$ ions. Similar removal of lattice distortion is known to occur in $MO_{3-x}F_x$ (M = Mo or W) systems.[12-14] Possible crystallographic relationships between unit

TABLE 1

Preparative and crystallographic data of $Ln_2Mo_3O_9$ defect scheelites

Ln	Formation temperature (*T*/K)	% Weight loss [a]	Oxidation state of Mo	Unit-cell parameters [b] a_T/Å	c_T/Å	c_T/a_T	U/Å³
La	800	6.20 (6.33)	4.04	5.35(6)	12.0(1)	2.24	343
Pr	790	6.37 (6.30)	3.97	5.30(6)	11.6(1)	2.20	326
Nd	780	6.40 (6.25)	4.01	5.28(5)	11.6(1)	2.19	322
Sm	870	6.15 (6.15)	4.04	5.24(3)	11.30(7)	2.16	310
Gd	850	5.90 (6.04)	4.06	5.19(2)	11.21(5)	2.16	302
Tb	840	5.98 (6.02)	3.96	5.14(1)	11.17(3)	2.17	295
Dy	830	6.05 (5.96)	3.95	5.13(1)	11.12(2)	2.17	292

[a] Values calculated for the reaction $Ln_2Mo_3O_{12} + 3\ H_2 \longrightarrow Ln_2Mo_3O_9 + 3\ H_2O$ are given in parentheses. [b] E.s.d.s are given in parentheses.

TABLE 2

X-Ray powder-diffraction data ($d_{obs.}$/Å) * of $Ln_2Mo_3O_9$ defect scheelites

h	*k*	*l*	I/I_0	$Nd_2Mo_3O_9$	$Gd_2Mo_3O_9$	$Tb_2Mo_3O_9$	$Dy_2Mo_3O_9$
1	1	2	100	3.143 (3.134)	3.081 (3.072)	3.053 (3.045)	3.042 (3.036)
1	0	3	100	(3.113)	3.042 (3.033)	3.015 (3.015)	3.006 (3.004)
0	0	4	35	2.903 (2.889)	2.808 (2.802)	2.790 (2.793)	2.777 (2.780)
2	0	0	40	2.637 (2.638)	2.600 (2.597)	2.571 (2.569)	2.562 (2.562)
2	0	4	30	1.949 (1.948)	1.903 (1.905)	1.889 (1.891)	1.884 (1.884)
1	1	6	10	1.710 (1.711)	1.665 (1.665)	1.658 (1.657)	1.650 (1.650)
3	1	2	15	1.621 (1.625)	1.576 (1.576)	1.560 (1.560)	1.556 (1.556)

* Calculated values are given in parentheses.

cells of the parent $Ln_2Mo_3O_{12}$ and the product $Ln_2Mo_3O_9$ are shown in Figure 4.

The $Ln_2Mo_3O_9$ phases may, therefore, be regarded as

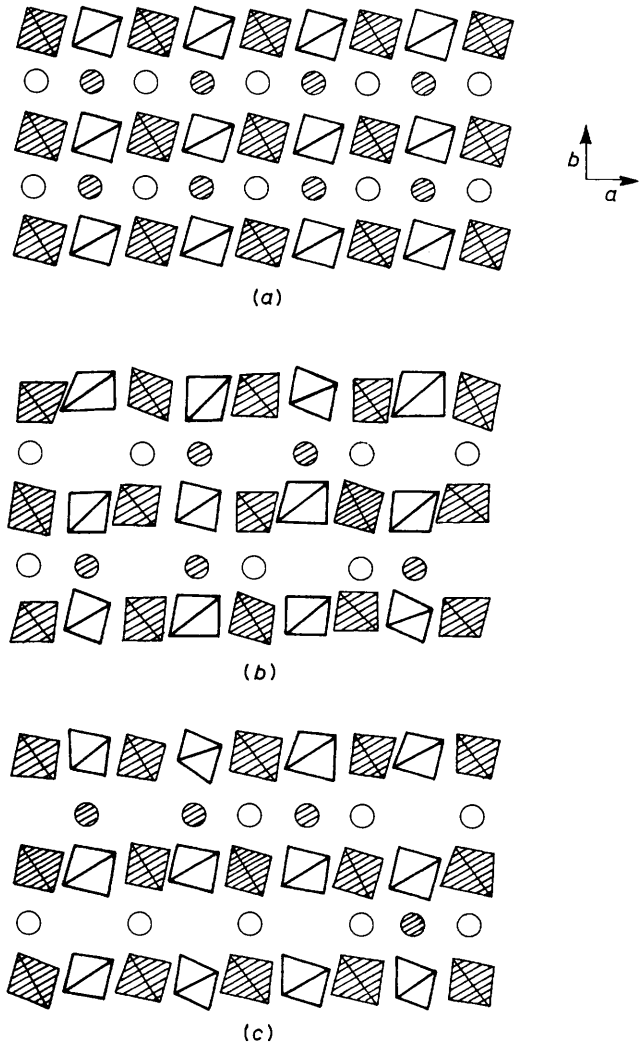

FIGURE 3 Structures of α-$Ln_2Mo_3O_{12}$ in relation to ideal ABO_4 scheelite structure projected down the *c* axis. The shaded circles and tetrahedra represent A site ions and BO_4 groups respectively at $Z = 0$ and the unshaded ones those at $Z = \frac{1}{4}$: (*a*) ideal scheelite; (*b*) α-$Gd_2Mo_3O_{12}$ (M type); and (*c*) α-$Nd_2Mo_3O_{12}$ (N type) (after refs. 4 and 10)

defect scheelites having one third of the A sites and a quarter of the anion sites vacant: $Ln_{2/3}(\square cat)_{1/3}MoO_3(\square an)$. The fact that there are no superstructure reflections in the *X*-ray patterns indicates that the anion vacancies are distributed at random. It is likely that these are frozen in the parent structure because of the fairly low temperatures at which reduction occurs. Hence these are metastable phases which are kinetically stabilized under the preparative conditions. On annealing in sealed evacuated silica tubes at 1 250 K, they

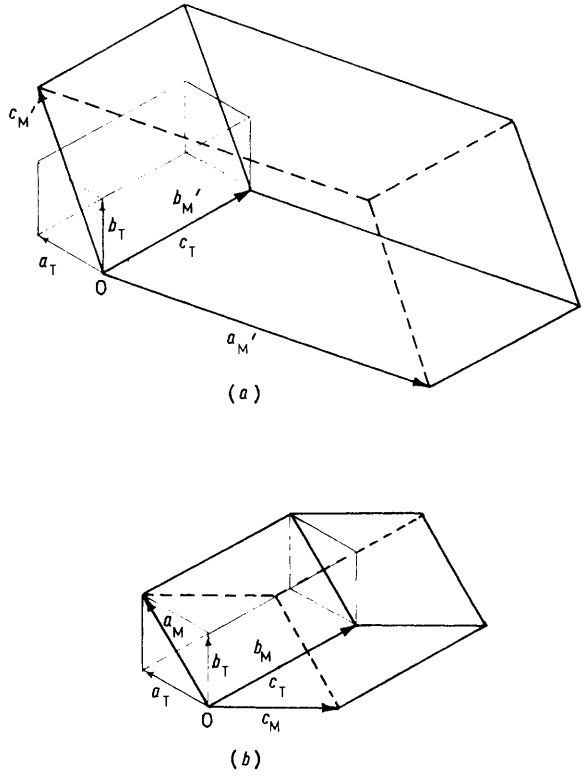

FIGURE 4 Relationship between the unit cells of (*a*) monoclinic $Nd_2Mo_3O_{12}$ (N structure) and tetragonal $Nd_2Mo_3O_9$, and (*b*) monoclinic $Gd_2Mo_3O_{12}$ (M structure) and tetragonal $Gd_2Mo_3O_9$

disproportionate to a mixture [7,15] of either $Ln_2Mo_2O_7$ and MoO_2 (Ln = La, Pr, Nd, or Sm) or Ln_2MoO_5 and MoO_2 (Ln = Gd, Tb, or Dy), indicating that $Ln_2Mo_3O_9$ are not stable equilibrium phases in the Ln_2O_3–MoO_2 system.

Infrared Spectra.—The i.r. spectra of $Ln_2Mo_3O_{12}$ and $Ln_2Mo_3O_9$ in the region 400—1 200 cm^{-1} (Figure 5) were recorded in order to distinguish the reduction products from the parent $Ln_2Mo_3O_{12}$ oxides.

The $A^{II}Mo^{VI}O_4$ scheelite oxides, having S_4 site sym-

metry for the MoO_4^{2-} group, show two absorption bands in this region, around 820 and 420 cm^{-1}, which correspond respectively to the ν_3 and ν_2 modes of the tetrahedral MoO_4^{2-} group.[16,17] In the scheelite-related

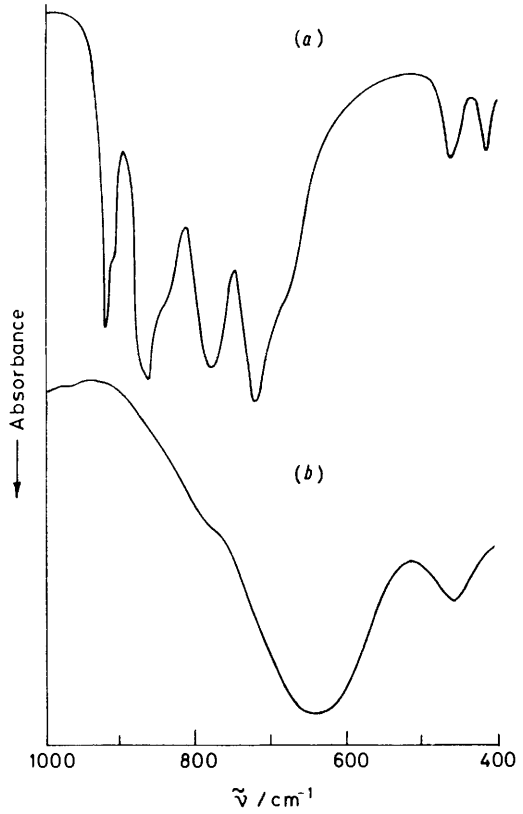

FIGURE 5 Infrared spectra of (*a*) α-$Gd_2Mo_3O_{12}$ and (*b*) its reduction product $Gd_2Mo_3O_9$

α-$Ln_2Mo_3O_{12}$ oxides the ν_3 and ν_2 modes are split into three and two components respectively. In addition, the ν_1 mode of MoO_4^{2-} which is i.r. inactive in the scheelite becomes active in $Ln_2Mo_3O_{12}$, occurring around 910 cm^{-1}. These differences between the spectra of the tetragonal scheelite and the monoclinic $Ln_2Mo_3O_{12}$ may be attributed to a further lowering of the site symmetry of the MoO_4^{2-} group in $Ln_2Mo_3O_{12}$.

The i.r. spectra of the tetragonal scheelite-related

TABLE 3

Electrical and magnetic data of $Ln_2Mo_3O_9$ defect scheelites

Ln	10^4 Conductivity at 300 K/ S cm^{-1}	Activation energy/ eV	Seebeck coefficient/ μV K^{-1}	Effective magnetic moment */ B.M.
La	5.0	0.19	−60	0.56
Pr	3.5	0.18	−40	3.70
Gd	10.0	0.16	−35	7.85
Tb	20.0	0.13	−45	9.80

* Per $LnMo_{3/2}O_{9/2}$ unit.

$Ln_2Mo_3O_9$, on the other hand, show two broad absorption bands centred around 640 and 460 cm^{-1}. These spectra are distinctly different from those of $Ln_2Mo_3O_{12}$ (Figure 5), no splitting of ν_3 and ν_2 being observed and the ν_1 mode is absent. However, it is difficult to assign the bands as arising from tetrahedral MoO_4 groups in view of the presence of random oxygen vacancies in $Ln_2Mo_3O_9$ which would render ill defined the molybdenum–oxygen polyhedra.

Electrical and Magnetic Properties.—Electrical conductivity measurements were made in the temperature range 300—700 K and the data are given in Table 3. It is seen that these phases are n-type semiconductors having activation energies around 0.15 eV.* The magnetic susceptibility measurements were carried out in the temperature range 80—300 K. The χ_m^{-1}–T plots (Figure 6) for Ln = Pr, Gd, and Tb are linear above 120 K indicating Curie–Weiss law behaviour. The effective magnetic moments obtained per $LnMo_{3/2}O_{9/2}$ unit (Table 3) reveal that the moment arises mainly from the lanthanide ions, the contribution from Mo^{4+} being small. The lanthanum compound shows a small $\mu_{eff.}$ (0.45 B.M. per $La_{2/3}MoO_3$) which is considerably

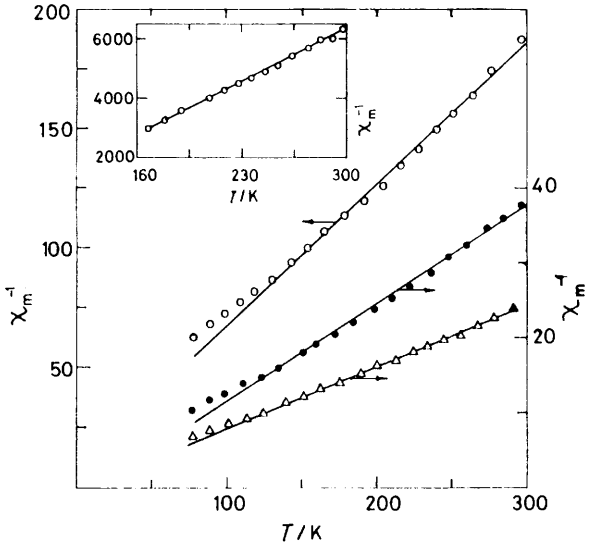

FIGURE 6 Variation of inverse molar magnetic susceptibility of $Ln_2Mo_3O_9$ defect scheelites with temperature: ○, $Pr_2Mo_3O_9$; ●, $Gd_2Mo_3O_9$; △, $Tb_2Mo_3O_9$. The variation of χ_m^{-1} of $La_2Mo_3O_9$ with temperature is shown in the inset

smaller than the value found in molybdenum(IV) compounds [18] in which the Mo^{4+} ions are far apart. This indicates that there is probably a strong Mo^{4+}–Mo^{4+} interaction in these phases.

The authors are grateful to Professor C. N. R. Rao for his keen interest and encouragement and for providing facilities for this work. A. M. is thankful to the Council of Scientific and Industrial Research, Government of India, for the award of a Research Fellowship.

[0/754 *Received*, 19*th May*, 1980]

* Throughout this paper: 1 eV ≈ 1.60 × 10^{-19} J; 1 B.M. ≈ 9.27 × 10^{-24} A m^2.

REFERENCES

[1] A. Manthiram and J. Gopalakrishnan, *J. Less-Common Met.*, 1979, **68**, 167.

[2] K. Nassau and J. W. Shiever, ' Solid State Chemistry,' NB

Special Publication No. 364, eds. R. S. Roth and S. J. Schneider, jun., U.S. Dept. Commerce, Washington D. C., 1972, p. 445.
[3] L. H. Brixner, *Rev. Chim. Miner.*, 1973, **10**, 47.
[4] A. W. Sleight, ' Advanced Materials in Catalysis,' eds. J. J. Burton and R. L. Garten, Academic Press, New York, 1977, p. 181.
[5] K. Nassau, H. J. Levinstein, and G. M. Loiacona, *J. Phys. Chem. Solids*, 1965, **26**, 1805.
[6] L. H. Brixner, P. E. Bierstedt, A. W. Sleight, and M. S. Licis, *Mater. Res. Bull.*, 1971, **6**, 545.
[7] A. Manthiram and J. Gopalakrishnan, *Proc. Indian Acad. Sci., Sect. A*, 1978, **87**, 267.
[8] R. D. Shannon, *Acta Crystallogr., Sect. A*, 1976, **32**, 751.
[9] K. Nassau, P. B. Jamieson, and J. W. Shiever, *J. Phys. Chem. Solids*, 1969, **30**, 1225.
[10] W. Jeitschko, *Acta Crystallogr., Sect. B*, 1973, **29**, 2074.
[11] J. M. Thomas, *Philos. Trans. R. Soc. London, Ser. A*, 1974, **277**, 251.
[12] A. W. Sleight, *Inorg. Chem.*, 1969, **8**, 1764.
[13] J. S. Anderson, ' Surface and Defect Properties of Solids,' eds. M. W. Roberts and J. M. Thomas, The Chemical Society, London, 1972, vol. 1, p. 13.
[14] R. J. D. Tilley, ' Crystallography and Crystal Chemistry of Minerals with Layered Structures,' ed. F. Levy, D. Reidel, Dordrecht, 1976, p. 137.
[15] A. Manthiram and J. Gopalakrishnan, *Indian J. Chem.*, in the press.
[16] R. G. Brown, J. Denning, A. Hallet, and S. D. Ross, *Spectrochim. Acta, Part A*, 1970, **26**, 963.
[17] R. A. Nyquist and R. O. Kagel, ' Infrared Spectra of Inorganic Compounds,' Academic Press, New York, 1971, p. 331.
[18] B. N. Figgis and J. Lewis, *Prog. Inorg. Chem.*, 1964, **6**, 123.